CROATICA CHEMICA ACTA CCACAA **69** (3) 1039–1052 (1996)

ISSN-0011-1643
*CCA–2361*

*Original Scientific Paper*

# Scanning Tunneling Microscopy of Surface Structures

*Velibor Marinković*

*Department of Materials and Metallurgy, Faculty of Natural Sciences and Technology, University of Ljubljana and J. Stefan Institute, SI-1000 Ljubljana, Slovenia*

Received April 26, 1996; revised May 29, 1996; accepted June 26, 1996

Surface science got a new impact with the development of the scanning tunneling microscope, since for the first time atomic-resolution observations of surface structures in real space have become possible. Following a short description of the basic features of the scanning tunneling microscopy, some selected results are presented which illustrate the potential of the technique to provide information about the surface structures and processes on a nanometer scale.

## INTRODUCTION

Since its invention by Binnig and Rohrer in 1981, scanning tunneling microscopy (STM) has found wide application in many fields of scientific research. However, up till now, STM has certainly had its greatest impact in the field of surface science. One of the first successes in this field was the solution of the atomic arrangement of the $(7 \times 7)$ reconstruction on Si (111) surface by the first real space imaging with atomic resolution.[1] Since then, numerous structures of clean and adsorbate-covered surfaces have been solved.

The surface structure has a dominant role in many surface processes, in the course of which it is often modified. Such processes can be studied by STM as a typical local microscopy probe which can characterize the surface structure of the initial and final states, and in some cases even its dynamic modification. The ability of local observation in combination with atomic scale resolution makes STM most suitable for the characterization of mostly local phenomena and structures of interest, as demonstrated in a number of studies.

In the case of an existing long-range order, diffraction methods normally yield more exact values of lattice parameters in the surface plane than it can be determined from STM images. However, STM can contribute very

useful additional information on the arrangement of atomic species in the large two-dimensional unit cells on reconstructed surfaces, for which the analysis of diffraction data is difficult. The most important advantage of STM with regard to surface diffraction methods is the possibility of obtaining atomically resolved information on real structures with deviations from long-range order. Thus, for example domain boundaries, locally ordered or disordered parts of the surface can be observed, and statistically distributed atomic defects can be resolved.

Various examples of layered crystal, metal, and reconstructed semiconductor surface studies will illustrate the STM ability.

## PRINCIPLES OF STM OPERATION

STM is in principle a tunneling junction, one electrode of which (in an ideal case) is an atomically sharp tip while the other is the studied surface itself. Under an applied voltage, a tunneling current results due to the overlap of exponentially decaying electron states of both electrodes. The net current across the tunneling gap will vary exponentially with the varying tip-sample distance, according to the relation:

$$I \approx \frac{V}{z} \exp(-Kz\sqrt{\phi}) \tag{1}$$

where $z$ is the width and $\phi$ the height of the potential barrier, and $K$ is a constant. The direction of electron flow depends on the polarity of the sample (sample bias). For negative sample biases, electrons tunnel from filled electronic states in the sample to empty states in the tip, while for positive sample biases electrons tunnel from filled states in the tip to the empty states in the sample (Figure 1). Thus, depending on the sign of the sample bias, either filled or empty electronic states in the sample can be probed. Relation (1) follows from the simplest planar electrode model for the tunneling microscope in which plane waves are scattered by an one-dimensional rectangular potential barrier. Since the tip and the sample may have different work functions, and since the sample is biased at a voltage $V$ relative to the tip, tunneling takes place through a trapezoidal barrier. It has been shown[2] that the barrier height in Eq. (1) can for $\bar{\phi} << eV$ be replaced by the effective barrier height given by

$$\bar{\phi} = \frac{1}{2}\left[\phi_{\text{tip}} + \phi_{\text{sample}} - |eV|\right] \tag{2}$$

In the tunneling microsope (Figure 2), the tunneling current is electronically stabilized by means of a feedback circuit, which regulates the sample-tip distance $z$ to a constant value. The actual $z$ value supplied by the feedback cir-

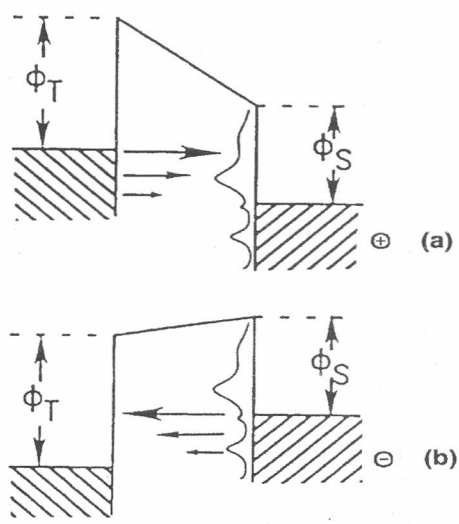


Figure 1. Relative energy levels for the positive (a) and negative (b) sample bias. In (a) the tip Fermi level is maintained at an energy eV above that of the sample by means of an applied bias and electrons tunnel from the tip to the sample, in (b) the situation is reversed. $\phi_T$ and $\phi_S$ are tip and specimen work functions.

cuit while scanning the tip over the sample surface may be used to construct an image of the surface. Such an image is called a constant current topograph (CCT).

The above simple model may be satisfactory for interpretation of low resolution STM images. However, it is far from adequate for images with atomic resolution, since it assumes a potential barrier independent of the $xy$ coordinates. The lateral variation of the potential barrier is defined by

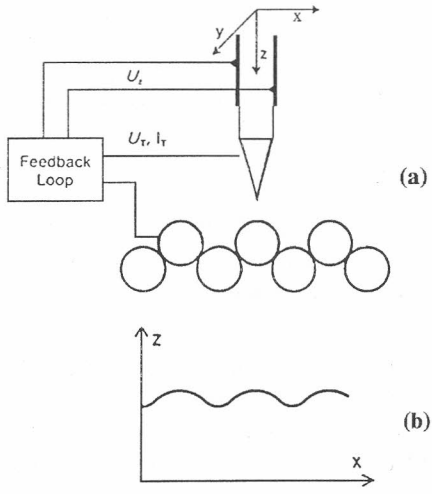


Figure 2. Schematic drawing of the STM set-up (a). A STM image is obtained by scanning a sharp metal tip over the surface using a piezodrive. The tunneling current is held constant by a feedback loop which maintains the sample-tip distance at a constant value. The actual $z$ value supplied by the feedback circuit as the tip moves along the surface outlines the contours of the surface (b).

the atomic charge density of the surface. To include it, Tersoff and Hamman[3] derived on the basis of Bardeen's work,[4] the following expression for the tunneling current:

$$I \approx V\phi^2 R^2 \exp(-AR)\, D_t(E_F)\, \rho(r_0, E_F) \tag{3}$$

where $D_t$ is the density of states per unit volume of the tip, $R$ is the tip radius and $\rho(r_0, E_F)$ is the Fermi-level density of states of the sample, measured at the position corresponding to the centre of the tip curvature. This relation shows that the contour followed by the tip in the CC mode is essentially a contour of constant Fermi-level density of states of the sample. However, to get more realistic results, a STM theory must explicitly take into account the electronic structure of both the tip and the substrate. A fundamental aspect of the STM operation which determines the nature and the meaning of the STM images is that the electronic states of both electrodes (the filled ones of the negative and the empty ones of the positive electrode) are directly involved in the tunneling process.

## STM OF THE Si(111) 7 × 7 SURFACE RECONSTRUCTION

The »topographic« maxima in STM images of semiconductor surfaces are usually associated with surface dangling bonds. However, the STM images of semiconductor surfaces are generally bias voltage dependent, which means that, depending on their energy, certain bonds may be seen at some particular sample bias voltage but not at others. To gain a full insight into the surface structure, it is therefore necessary to perform voltage dependent STM studies.

This can be most appropriatelly illustrated by the Si(111) 7 × 7 surface structure.[5] The (7 × 7) reconstruction can be obtained by thermally annealing a crystal typically above 1200 K under ultra-high-vacuum conditions to remove the surface oxide layer by sublimation. By subsequent slow cooling to ambient temperature, the high temperature (1 × 1) surface structure is transformed at about 1130 K into the energetically more favourable (7 × 7) superstructure. The driving force for this (1 × 1) to (7 × 7) transformation is the reduction of dangling bond density. The number of dangling bonds per (7 × 7) unit cell is reduced to 19, as compared with 49 for the (1 × 1) surface structure.

STM images of the Si(111) 7 × 7 surface reveal 12 »topographic« maxima per unit cell, as shown in Figure 3, which can be attributed to the 12 dangling bonds of the 12 adatoms in the so-called DAS (dimer-adatom-stacking fault) model (Figure 4). According to the DAS model, proposed by Takayanagi *et. al.*[6] on the basis of transmission electron diffraction data, the (7 × 7) re-

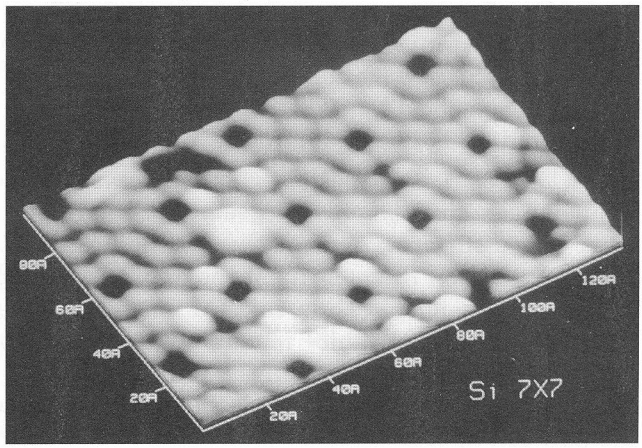


Figure 3. STM image of Si (1 × 1) 7 × 7 reconstruction. 12 adatoms are resolved inside each unit cell with characteristic holes at its 4 corners (Courtesy of the Omicron Application Laboratory).

construction affects 4 surface atomic layers. In the reconstructed unit cell with a vacancy at the corner (»corner hole«), 36 dangling bonds of the second atomic layer are saturated by 12 Si adatoms in the topmost layer. At the edges of both triangular subcells of the (7 × 7) unit cell, nine dimers are formed in the third atomic layer. Between the third and fourth atomic layers, a stacking fault is present in one half of the cell. The 19 dangling bonds per unit cell are located on the 12 adatoms, the six »rest-atoms« (triply coordinated silicon atoms), and on the atom at the bottom of the corner hole. Since the dangling bonds of the adatoms are partially filled, they contribute to both empty and filled states. While other structural models proposed for

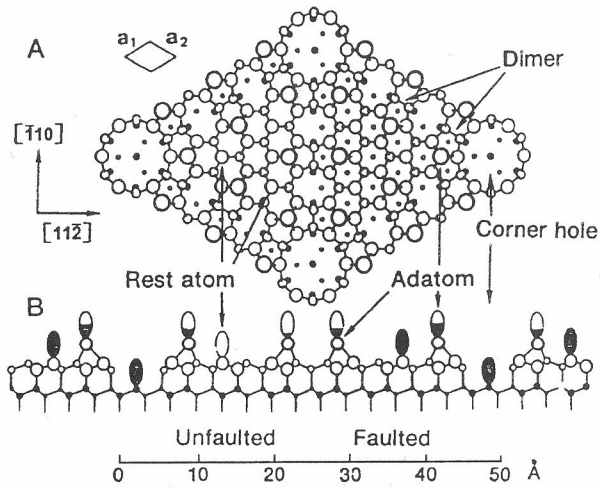


Figure 4. DAS model of the Si(111) 7 × 7 surface according to Takayanagi *et al.*,[6] top view (a), and side view (b). The reconstruction which affects 4 surface atomic layers reduces the number of dangling bonds from 49 of the (1 × 1) surface structure to 19. They are located on the 12 adatoms, 6 rest-atoms and on the atom at the bottom of the corner hole.

the Si(111) $7 \times 7$ structure failed to fit the experimental STM data satisfactorily, the STM images of the Si(111) $7 \times 7$ structure were found to be in excellent agreement with the DAS model. Although the Si(111) $7 \times 7$ structure has not been solved by STM, it has certainly significantly contributed to the discrimination between different structural models.

Si(111) $7 \times 7$ is a special example of a semiconductor surface for which STM images directly provide geometric information about the lateral positions of the surface atoms. Although the positions of the observed maxima do not depend on the polarity of the applied bias voltage, the image contrast is polarity dependent. Thus, in STM images obtained with a positive sample bias, the 12 »topographic« maxima are of equal brightness, indicating an equal height of all adatoms in the unit cell (Figure 3), while in STM images obtained with a negative sample bias, the 6 adatoms in the faulted half of the unit cell appear »higher« than those in the unfaulted half. This indicates significant electronic contributions to the observed image contrast. However, in the case of Si(111) $7 \times 7$, the electronic effects influence only determination of the $z$ position of the adatoms, while their $xy$ coordinates may be directly determined from the CCT. In general, however, the apparent atomic positions in CCTs do not always correspond to that of the atoms, as *e.g.* shown[7] for Si(100) $2 \times 1$ and in several other cases.

Additional information on electronic effects in STM images of the Si(111) $7 \times 7$ surface has been obtained by local tunneling spectroscopy measurements.[5] The conductance curves ($I/U$ *versus* $U$) measured at different specific locations within the reconstructed unit cell show maxima at particular bias voltages corresponding to the energies of the surface states. At the energies of surface states, symmetry changes are observed in STM current images. In this way, the atomic origins of various electronic states can be directly determined. This ability to map out the electronic surface states with a lateral resolution of about 0.3 nm is a unique feature of the STM technique, which can be used to study surface chemistry with atomic resolution.

## LAYERED CRYSTALS

Layered crystals like those of transition metal dichalcogenides (TMD) possess a variety of properties that make them very interesting and suitable objects for STM studies. TMD crystals are built by neutral three-layer chalcogen-metal-chalcogen sandwiches, which are held together only by weak van der Waals bonds. Their easy cleavage across the van der Waals gaps between the TMD sandwiches results in large atomically flat terraces, which are ideally suited to atomic resolution studies by STM.

The strong two-dimensional character of TMD crystals, which increases from Group-VI to Group-IV transition metal compounds, is also expressed

in temperature dependent anisotropic physical properties, often accompanied by anomalies. In Ta and Nb dichalcogenides charge-density waves (CDWs) trigger periodic structural distortions.[8] Their periodicity and orientation are not only temperature dependent but, in general, also incommensurate with the underlying lattice. Although CDWs were intensively studied in the past,[8] the appearance of STM opened new possibilities in direct observation of surface CDWs and atomic displacements. In a recent detailed STM study,[9] a series of TMD crystals was studied at different temperatures and it was shown that CDWs with largest and smallest amplitudes appear in 1T and 2H compounds, respectively, while compounds with mixed stackings exhibit intermediate amplitudes. In a comparative STM study of $NbSe_2$, $TaS_2$ and 3R-$Nb_{1+x}S_2$ crystals,[10] we have shown that contrary to the well ordered $NbSe_2$ surface and a strong nearly commensurate CDW modulation on $TaS_2$, both in agreement with earlier observations, the $Nb_{1+x}S_2$ surface displayed an irregularly fluctuating corrugation with the periodicity of the $NbS_2$ lattice (Figure 5). In the 3R-$Nb_{1+x}S_2$, the surplus Nb atoms self-intercalate into van der Waals gaps.[11] Thus, the observed irregularity could be caused either by Nb atoms remaining on the observed surface after cleavage or by Nb atoms in the first subsurface van der Waals gap. These could cause a short-range charge variation along the topmost Nb layer, or a pure atomic accommodation of the surface S layer. Since STM is only exceptionally able to discriminate between different chemical species, it is difficult to ascertain the proper cause of the observed surface disorder.

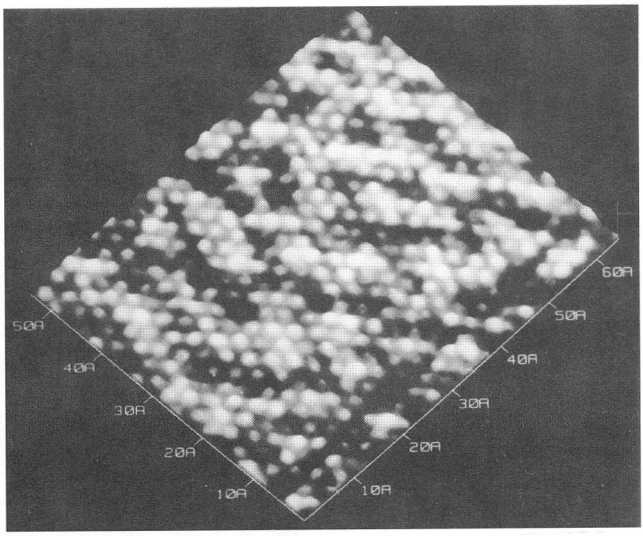


Figure 5. Irregular corrugations on a 3R-$Nb_{1+x}S_2$ (001) face caused by self-intercalated surplus Nb atoms.[10]

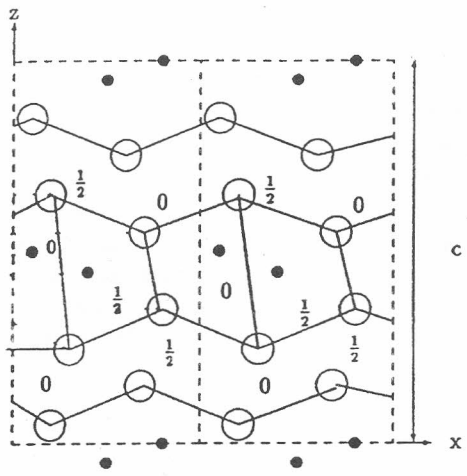


Figure 6. A (010) projection of the $WTe_2$ structure. Large open circles – Te atoms, small filled circles – W atoms, their $y$ coordinates, either 0 or 1/2, are indicated. Alternate Te rows parallel to the [010] direction differ in height by 0.06 nm, thus forming troughs and ridges on the (001) cleavage face of the crystal.

In several papers on STM observations of atomically resolved images of TMD cleavage faces, it has been argued that the images represent subsurface metal layers rather than the top chalcogen ones.[12–14] Since in TMD crystals with hexagonal symmetry, both metal and chalcogen layers have the same symmetry and in-plane interatomic distances, it is difficult to decide which atoms are mainly contributing to the STM images. A possibility to clarify this problem is offered by β-$MoTe_2$ and $WTe_2$ crystals, in which the atomic arrangements in Te and metal layers are different (Figure 6). The first principles pseudopotential calculation result on $WTe_2$ shows[15] that the charge distribution of the topmost Te atoms is shifted toward the metal at-

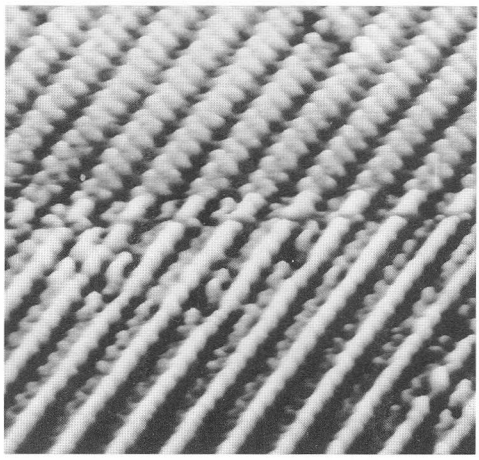

Figure 7. STM topograph (8 nm × 8 nm) of the β-$MoTe_2$ (001) surface. In the lower half of the topograph rows of the Te surface atoms are imaged, while the upper half corresponds to the arrangement of subsurface Mo atoms.[16]

oms causing a W-layer-like image. According to this calculation, the charge displacement occurs only at the negative sample bias, while for the positive sample bias, the charge distribution is almost centered at the actual atomic positions. This is however, in disagreement with the experiments[15] where the same kind of images were obtained with both sample biases. In contrast to these, our STM images of β-$MoTe_2$ (Figure 7) show details which, depending on the tip electronic condition, resemble the atomic arrangements of either the topmost Te or the subsurface metal layers.[16] In the later case, the $d_{z^2}$ orbitals of metal atoms protruding vertically upward may provide the tunneling current.

Due to the atomic flatness of the cleavage faces of the majority of TMD crystals, they are also suitable substrates for studies of nucleation and growth of various deposits. The existence of periodically corrugated cleavage faces in some of these crystals, like in the already mentioned β-$MoTe_2$ and $WTe_2$, makes it possible to study the influence of different surface topographies of chemically closely related or even identical (*e.g.* α- and β-$MoTe_2$) substrates in the initial stages of thin film growth. We have compared the growth of Au on buckled (001) faces of $WTe_2$ and β-$MoTe_2$ with its growth on smooth (001) α-$MoTe_2$ faces.[17,18] On all three crystals, Au grows in the form of islands, isotropically shaped on α-$MoTe_2$, and elongated and aligned along [010] Te ridges on the buckled faces of the other two crystals. The smallest gold clusters that could be observed by STM on (001) $WTe_2$ simultaneously with the resolved substrate Te rows were about 0.3–0.4 nm wide and 3–4 nm long (Figure 8). While Au grows on α-$MoTe_2$ with its close-packed planes and directions parallel to those of the substrate crystal, the orientation relationship on the buckled faces was found to be (112)[1$\bar{1}$0]Au || (001)[010]$WTe_2$ or β-$MoTe_2$. It was shown that on

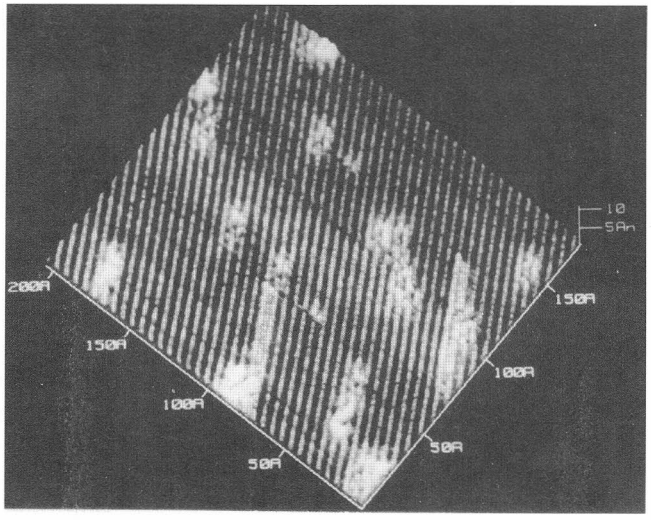


Figure 8. Nucleation of vacuum deposited gold on $WTe_2$ (001) surface.[18] Note the elongated gold islands along the substrate Te ridges.

the buckled faces Au forms 1D nuclei due to enhanced diffusion along surface troughs, and that the observed orientation was a consequence of similar atomic topographies of (112) Au and (001) substrate planes. These results show that differences in surface topography can have an important role in the growth of metal deposits on chemically similar surfaces with low surface free energies.

## EPITAXIAL GROWTH ON SEMICONDUCTOR SURFACES

The initial stages of growth of thin overlayers on various substrates profoundly influence their further growth, and thus their stucture and properties. STM studies of the initial stages of growth of thin metal overlayers on semiconductor substrates can provide valuable information on the structure and properties of the metal-semiconductor interfaces needed *e.g.* for a better understanding of Schottky barrier formation. However, in these studies there is often a problem of assigning the observed surface protrusions in STM topographs to specific atomic species without additional information from other surface analytical techniques.

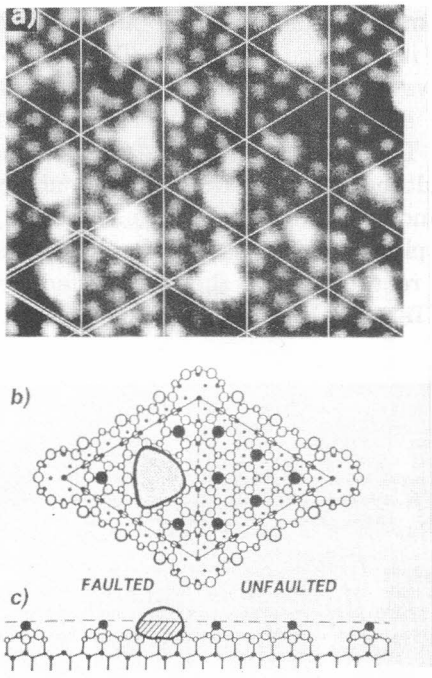


Figure 9. STM topograph of an 11.5 nm × 9.5 nm area of Si(111) 7 × 7 surface covered with 0.25ML of Pd (a).[8] The Pd-silicide clusters have nucleated preferentially within the faulted half of the (7 × 7) unit cell, as shown schematically in (b) and (c).

STM is, on the other hand, ideally suited to study spatially selective nucleation phenomena. Preferential nucleation of two-dimensional metal islands on the faulted halves of the (7 × 7) unit cells has been observed for condensation of Cu, Ag, and Pd[19] on a Si(111) 7 × 7 substrate. In the case of Pd, 95% of the nucleated islands were found to be located on the faulted halves of the (7 × 7) structure (Figure 9). These results reveal for the first time that the difference in electronic and atomic structures of a subsurface stacking fault with regard to the unfaulted structure can influence the adsorption of adatoms.

STM as a local probe can be particularly useful in cases where several different surface phases coexist, as *e.g.* after deposition of half a monolayer (ML) of tin on Si(111) $7 \times 7$, where three different surface structures ($7 \times 7$, $\sqrt{3} \times \sqrt{3}$, and $2\sqrt{3} \times 2\sqrt{3}$) can be observed simultaneously.[20] It is evident that surface analytical techniques which collect data by averaging over large surface areas are not able to provide correct information about the atomic and the electronic structure of such inhomogeneous surfaces with particular surface phases extending over areas only a few nanometers in diameter.

From a technological point of view, Si(100) is one of the most important surfaces, since most integrated circuits are made on it. In the LEED experiments, a $(2 \times 1)$ diffraction pattern is observed, which indicates a reconstruction with a doubled periodicity in one direction. It follows unambiguously from a high-resolution STM study[21] that from several proposed models the dimer model is the correct one. In the bulk-like terminated surface, each of the top-layer atoms is bonded to two atoms in the second layer, leaving two dangling bonds on each top-layer atom. Pairs of these atoms dimerize, leaving only a single dangling bond per surface atom. The resulting $(2 \times 1)$ unit cell, therefore, contains two dangling bonds.

Of great technological interest are also STM studies of the step structure of vicinal Si(100) surfaces (Figure 10) and of the epitaxial growth on such

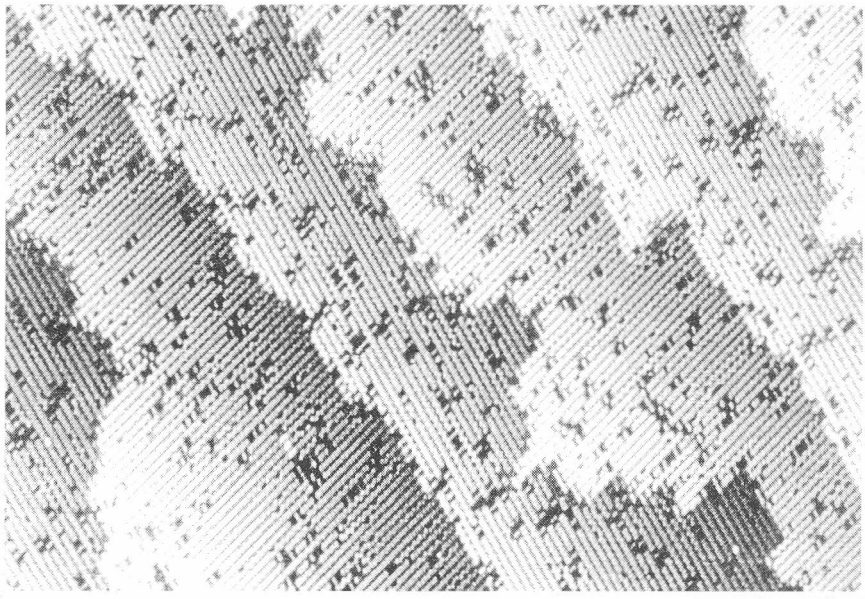

Figure 10. STM image of a 58 nm × 86 nm area of a stepped Si(001) $2 \times 1$ surface[11] with two types of steps and numerous vacancy-type defects.

surfaces. For miscut angles of 2° or less, the steps are predominantly of monoatomic height.[22] As a consequence of the diamond-type crystal structure of silicon, the dimer rows of (2 × 1) reconstruction are rotated by 90° on going from one terrace to the next. The separation of dimer rows is 0.768 nm; the dimers within rows are half this distance apart, and the atoms in each dimer are separated by about 0.24 nm. The atoms in the dimer cannot be resolved. With regard to the orientation of the dimer rows on the upper terrace relative to the step edges, two different types of steps are distinguished: parallel A-type steps, and perpendicular B-type steps. If the equilibrium step structure was reached during surface preparation, the A-type steps were found to be rather smooth, whereas B-type steps appeared rough with many kink sites (Figure 10).

Since the surface diffusion of adatoms is fundamentally important in epitaxial growth, atomic-scale observations of surface migration by STM have been performed for Si adatoms on top of Si(100) 2 × 1 substrates.[23] It was found that the dimer-type (2 × 1) reconstruction of the Si(100) surface leads to a strong anisotropy in the surface diffusion process, which is about 1000 times faster along the surface dimer rows than perpendicular to them. Thus, at early stages in the epitaxy of Si on Si(100) 2 × 1 below 625 K, anisotropic islands have been observed, with the long direction of each island along the dimer-bonding direction of the underlying layer. Upon annealing, the shapes of the islands become more isotropic, indicating that the initially formed anisotropic islands represent, to a large degree, non-equilibrium growth structures.

Since STM is also a powerful tool for characterization of non-periodic surface structures, such as defects, their influence on surface processes, *e.g.* epitaxial growth, chemical reactions, etc. can be studied in detail on a local scale. The density of defects on the Si(100) 2 × 1 surface (Figure 10) is typically higher than on the Si(111) 7 × 7 surface for the same preparation conditions. Besides single and double dimer vacancy-type defects another type of characteristic defect, the so called »C-defect«, could also be distinguished.[22]

In several adatom-substrate systems, the adatoms occupy substitutional sites in the reconstructed surface rather than lie on top of it. Atomic-scale studies of surface diffusion have been performed of isolated, randomly distributed Pb adatoms occupying substitutional sites on the reconstructed Ge(111)c(2 × 8) surface.[24] The Pb and Ge adatoms are distinguishable over a range of biases, which allows observation of how the Pb adatoms change their positions on the surface. Adatom interchanges between nearest-neighbour sites, as well as over longer distances were observed. For the nearest-neighbour interchanges, the diffusion appears to be anisotropic within a single c(2 × 8) domain. From STM studies between 300 and 350 K, an activation energy of 0.54 eV was determined for the diffusion of Pb adatoms.

## CLEAN AND ADSORBATE-COVERED METAL SURFACES

Due to the delocalized character of s- and p-type states, which are usually probed in metals by STM, the measured corrugation amplitudes for non-reconstructed metal surfaces are only of about 0.01 nm height. While a pronounced bias-voltage dependence is usually not observed in STM topographs of clean metal surfaces, the STM images of adsorbate-covered surfaces are again strongly bias-dependent, like in the case of semiconductor surfaces.

STM studies of metal surfaces were stimulated by the first atomically resolved images of the close-packed Au(111) surface,[25] of special interest as the only reconstructing (111) FCC metal surface. STM observation of two bright stripes within the $(23 \times \sqrt{3})$ reconstructed unit cell, in addition to the underlying atomic lattice[26] is consistent with a stacking-fault-domain model involving periodic transitions between surface regions with FCC- and HCP-type stacking of top layers, induced by surface elastic strain. The parallel corrugations along the $[11\bar{2}]$ direction represent transition regions between HCP and about twice wider FCC domains. In accordance with the threefold symmetry of the (111) Au surface, three rotational variants of the less symmetrical $(23 \times \sqrt{3})$ reconstruction are observed simultaneously in larger areas. These rotational domains often form a long-range superstructure consisting of a correlated periodic bending of the parallel corrugation lines by 120°.

Only a few STM investigations of ordered metal alloys were reported. An interesting example is the $Pt_{25}$ $Ni_{75}$ (111) surface, which allowed the first clear STM discrimination of two chemical species in a metal alloy.[27] This discrimination is supposed to be caused by special tunneling conditions, attributed to an adsorbate at the STM tip, causing a difference in corrugation between Pt and Ni atoms of 0.03 nm. The STM data revealed a chemical short-range order at the surface in agreement with embedded atom simulations and can be understood as small domains of an $L1_0$ ordered phase.

Adsorption of oxygen, motivated by the desire to understand the initial stages of metal oxide formation has been studied for a variety of metal substrates. Most STM studies of oxygen adsorption have concentrated on Cu substrates. Of interest is also how a preadsorbed oxygen adlayer influences the homoepitaxial growth of metal. Thus, the growth of Ni on a clean Ni(100) surface proceeds at 300 K and 0.3 ML/min flux rate via homogeneous nucleation, lateral growth, and coalescence of two-dimensional, monolayered Ni islands, exhibiting an almost perfect layer-by-layer growth behaviour. The oxygen adlayer, which floats on the surface in its initial $c(2 \times 2)$ structure, has little effect on the growth mode and the actual growth process. However, it influences the dynamics of the 2D island growth, where the island edges are reoriented from along [011] on a clean surface to along [001] on an oxygen covered surface. This observation and the simultaneous change from a square to a pronounced rectangular island shape are explained in a simple picture based on the registry relation between O $c(2 \times 2)$ adlayers on two subsequent Ni layers.[28]

## REFERENCES


1. G. Binnig, H. Rohrer, Ch. Gerber, and E. Weibel, *Phys. Rev. Lett.* **50** (1983) 120–123.
2. J. G. Simmons, *J. Appl. Phys.* **34** (1963) 1793–1803.
3. J. Tersoff and D. R. Hamman, *Phys. Rev. B* **31** (1985) 805–813.
4. J. Bardeen, *Phys. Rev. Lett.* **6** (1961) 57–59.
5. R. J. Hamers, R. M. Tromp, and J. E. Demuth, *Phys. Rev. Lett.* **56** (1986) 1972–1975.
6. K. Takayanagi, Y. Tanishiro, S. Takahashi, and M. Takahashi, *Surf. Sci.* **164** (1985) 367–392.
7. R. M. Feenstra and M. A. Lutz, *Phys. Rev. B* **42** (1990) 5391–5394.
8. J. A. Wilson, F. J. DiSalvo, and S. Mahajan, *Adv. Phys.* **24** (1975) 117–202.
9. R. V. Coleman, B. Giambatista, P. K. Hansma, A. Johnson, W. W. McNairy, and C. G. Slough, *Adv. Phys.* **37** (1988) 559–644.
10. M. Remškar, A. Prodan, and V. Marinković, *Surf. Sci.* **287/288** (1993) 409–413.
11. W. G. Fisher and M. J. Sienko, *Inorg. Chem.* **19** (1980) 39–43.
12. G. W. Stupian and M. S. Leung, *Appl. Phys. Lett.* **51** (1987) 1560–1562.
13. S. Akari, M. Stachel, H. Birk, E. Schreck, M. Lux, and K. Dransfeld, *J. Microsc.* **152** (1988) 521–522.
14. S. L. Tang, L. Kasowski, and B. A. Parkinson, *Phys. Rev. B* **39** (1989) 9987–9991.
15. S. L. Tang, R. V. Kasowski, A. Suna, and B. A. Parkinson, *Surf. Sci.* **238** (1990) 280–288.
16. S. W. Hla, V. Marinković, A. Prodan, and I. Muevi, *Surf. Sci.* **352/354** (1996) 105–111.
17. R. Posel, V. Marinković, A. Prodan, and M. Remškar, Book of Abstracts, *15th European Crystallographic Meeting*, Dresden, 1994, p. 554.
18. S. W. Hla, V. Marinković, and A. Prodan, *Surf. Sci.* **356** (1996) 130–136.
19. U. K. Köhler, J. E. Demuth, and R. J. Hamers, *Phys. Rev. Lett.* **60** (1988) 2499–2502.
20. J. Nogami, S. I. Park, and C. F. Quate, *J. Vac. Sci. Technol. A* **7** (1989) 1919–1921.
21. R. M. Tromp, R. J. Hamers, and J. E. Demuth, *Phys. Rev. Lett.* **55** (1985) 1303–1306.
22. R. J. Hamers and U. K. Köhler, *J. Vac. Sci. Technol. A* **7** (1989) 2854–2859.
23. Y. W. Mo, J. Kleiner, M. B. Webb, and M. G. Lagally, *Surf. Sci.* **268** (1992) 275–295.
24. E. Ganz, S. K. Theiss, I. S. Hwang, and J. Golovchenko, *Phys. Rev. Lett.* **68** (1986) 1567–1570.
25. V. M. Hallmark, S. Chiang, J. F. Rabolt, J. D. Swalen, and R. J. Wilson, *Phys. Rev. Lett.* **59** (1987) 2879–2882.
26. J. V. Barth, H. Brune, G. Ertl, and R. J. Behm, *Phys. Rev. B* **42** (1990) 9307–9318.
27. M. Schmid, H. Stadler, and P. Varga, *Phys. Rev. Lett.* **70** (1993) 1441–1444.
28. E. Kopatzki, S. Günther, W. Nichtl-Pecher, R. J. Behm, *Surf. Sci.* **284** (1993) 154–166.


## SAŽETAK

### Tunelska mikroskopija površinskih struktura


*Velibor Marinković*



Razvoj tunelske mikroskopije dao je nov poticaj za studij površina, jer je po prvi put postalo ostvarivo razlučivanje na atomskoj skali. Nakon kratkog opisa osnovnih karakteristika tunelske mikroskopije prikazani su odabrani rezultati koji ilustriraju potencijal ove tehnike za dobivanje informacija o površinskim strukturama i procesima na nanometarskoj skali.